

# Pulse shape effects in qubit dynamics demonstrated on an IBM quantum computer

Ivo S. Mihov and Nikolay V. Vitanov

*Department of Physics, Sofia University, James Bourchier 5 blvd, 1164 Sofia, Bulgaria*

(Dated: January 25, 2023)

We present a study of the coherent interaction of a qubit with a pulse-shaped external field of a constant carrier frequency. We explore, theoretically and experimentally, the transition line profile — the dependence of the transition probability on the detuning — for five different pulse shapes: rectangular, Gaussian, hyperbolic-secant, squared hyperbolic-secant and exponential. The theoretical description for all cases but  $\text{sech}^2$  is based on the analytical solutions to the Schrödinger equation or accurate approximations available in the literature. For the  $\text{sech}^2$  pulse we derive an analytical expression for the transition probability using the Rosen-Zener conjecture, which proves very accurate. The experimental results are obtained with one of IBM's quantum processors. An excellent agreement between theory and experiment is observed, demonstrating some pulse-shape-dependent fine features of the transition probability profile. The divergence index — a measure of the accuracy of the fit — features an improvement by a factor of 4 to 7 for the analytic models compared to the commonly used (sinc<sup>2</sup> and Lorentzian) baseline fits. Moreover, we observe a reduction by about a factor of about 4 of the error bars of the resonance frequency of the qubit for the analytic models compared to the baseline fits. These results demonstrate both the accuracy of the analytic modelling of quantum dynamics and the excellent coherent properties of IBM's qubit.

## I. Introduction

Quantum algorithms promise to revolutionise the way we do certain operations like searching, counting, factoring, encrypting and transferring data, and even breaking some advanced encryption protocols. Quantum algorithms are constructed using quantum gates, which in turn are achieved by applying a pulse of microwave or laser radiation to the qubit. The behaviour of the qubit under different types of pulses is described by a number of models, each defined by the time dependence of the Rabi frequency  $\Omega(t)$  and the detuning  $\Delta(t)$  of the applied pulse. One common trait of all models is they predict the pulse area  $S = \int_0^T \Omega(t) dt$  must be equal to  $\pi$  for unit transition probability to state  $|1\rangle$ , assuming we start in state  $|0\rangle$  and we are exactly at resonance ( $\Delta = 0$ ).

In general, we can categorise the models in several ways. One option is to distinguish ones with constant or variable detuning. From another viewpoint, we can divide them into 3 different categories depending on the pulse shape: exponential, trigonometric and polynomial. Among the exponential models, we have the Rosen-Zener model [1], the Gaussian model [2], the Tanh model [3], and the Demkov model [4]. Among the trigonometric ones we have the powers-of-sine models [5] (e.g. the Sine model, the Sine-squared model etc.). The polynomial models include the Lorentzian-based models [6]. Note that the Rabi (rectangular) model [7] can be treated as a zeroth-order member of any of these categories, so it forms its own group.

Certain types of models assume pulses of infinite duration. Naturally, they are not exactly applicable in practice. However, they can be modified, so as to adopt a truncated version of the same type of pulse, leading to practical models with actual implications. Examples of such pulse types include the hyperbolic secant, Gaussian, Lorentzian and other infinite-duration shapes.

Other models have natural initial and final points and do not need truncation. This usually implies smaller dependence on the actual implementation of the model. Among these are the Rabi model, the Sine model, etc.

The pulse shape plays a key role in the functional form of the transition probability. Specifically, this affects the transition line profile  $P_{0 \rightarrow 1}(\Delta)$  — the dependence of the transition probability  $P_{0 \rightarrow 1}$  on the detuning  $\Delta$ . Although pulse shape effects on the qubit dynamics have been known for a long time, very few studies have directly verified them. Among these we note the significant reduction of power broadening in two-photon excitation by Gaussian pulses [8, 9] and a detailed study of pulse-shape effects on the Rabi oscillations [10].

We note that on exact resonance, the transition probability depends on the pulse area only and hence the ensuing Rabi oscillations do not depend on the pulse shape. It is off-resonance where the difference begins to emerge — the larger the detuning from resonance, the greater the differences. Hence, the most direct way to observe pulse-shape effects is to explore the transition line profile. This task is somewhat obstructed by the fact that for large detuning (much greater than  $1/\tau$ , the inverse pulse width) where the pulse-shape differences are most pronounced, the transition probability is very small and hard to measure. Nevertheless, measurable differences emerge even for small detuning (of the order of  $1/\tau$ ).

In this work, we will explore the notion that the pulse shape has a pronounced impact on the transition line profile. We study the transition probability for several exponential models of constant detuning, for which exact or approximate expressions for the transition probability are available — the Rabi, Rosen-Zener, Gaussian, and Demkov models. We add to these the Sech<sup>2</sup> model, for which the transition probability is derived here by using earlier conjectures. We compare the theoretical predictions with experimental results obtained by us using with

the IBMQ Armonk quantum processor [11]. Evaluating our custom divergence index (DI), we give a measure of the extent to which the theoretical models apply to the experimental measurements.

## II. Experimental method

The qubit performance is evaluated using the experimentally measured frequency responses for five different pulse shapes. Each of the transition profiles is fitted with an analytically calculated expression and also with a baseline function. The analytical expressions are calculated using the experimental values for the pulse width, duration and Rabi frequency, and then are post-processed to take into account the effects of the dephasing, readout and leakage errors of the qubit, see the text below. Furthermore, the fits are checked for overfitting by calculating an overfitting index using an average of the point-wise derivative of the experimental data points.

### A. Dephasing, readout and leakage errors

The post-processing procedure takes three effects — dephasing, readout error and population leakage to non-qubit states — into account in an empirical manner. Because these losses affect the qubit states differently, we set the transition probability as

$$P_{0 \rightarrow 1} = \epsilon_0 + (1 - \epsilon_0 - \epsilon_1)P_{0 \rightarrow 1}^{(0)} \quad (1)$$

where  $P_{0 \rightarrow 1}^{(0)}$  is the ideal transition probability in the completely coherent, lossless case, whereas  $\epsilon_0$  and  $\epsilon_1$  are free fitting parameters. Obviously, if  $P_{0 \rightarrow 1}^{(0)} = 0$ , we have  $P_{0 \rightarrow 1} = \epsilon_0$ , and if  $P_{0 \rightarrow 1}^{(0)} = 1$ , we have  $P_{0 \rightarrow 1} = 1 - \epsilon_1$ , i.e.,  $\epsilon_0$  accounts for the lifted background and  $\epsilon_1$  for the degradation of the probability from unity.

The modification of the transition probability of Eq. (1) was always applied, with  $P_{0 \rightarrow 1}^{(0)}$  taken from the theoretical expressions for the transition probability with no fitting parameters, and  $\epsilon_0$  and  $\epsilon_1$  determined by fitting to the experimental data.

### B. Fits and agreement between theory and experiment: Divergence and overfitting indices

The experimental data points  $P(\Delta)$  for each of the models executed in the experiment are fit to two different shapes — a model formula  $P_{0 \rightarrow 1}(\Delta)$  for each pulse shape and a baseline  $B(\Delta)$ . The model prediction is then compared to the baseline by finding the residuals  $R(\Delta)$  for some fit  $F(\Delta)$  as

$$R(\Delta) = F(\Delta) - P(\Delta). \quad (2)$$

Using Eq. (2) we calculate the divergence index (DI)

$$DI = \frac{1}{N} \sum_{i=1}^N |R(\Delta_i)| = \frac{1}{N} \sum_{i=1}^N |F(\Delta_i) - P(\Delta_i)| \quad (3)$$

where a larger DI signals greater discrepancy between the fit and the experimental data.

Sometimes fitting a function with many parameters to a small number of data points can lead to overfitting. This is a phenomenon where the fit describes the data very well, but does not generalise the behaviour well, as new data points have a large error.

To check whether we have overfitting we find the discrete derivative of the transition probability experimental points and take the absolute value, then take the mean to find the overfitting index (OFI), viz.

$$OFI = \frac{1}{N-1} \sum_{k=1}^{N-1} |P(\Delta_{k+1}) - P(\Delta_k)|. \quad (4)$$

We compare the OFI against a threshold value to conclude if we have overfitting. If the OFI is larger than the threshold, we identify overfitting and repeat the fitting process with new initial parameters given to the fit.

### C. Different Pulse Envelopes

Multiple pulse shapes are investigated in the experiment. Among them are three examples of exactly analytically soluble models — the Rabi [7], Rosen-Zener [1] and Demkov [4] models — and two models that only have approximate solutions: the Gaussian [2] and  $\text{sech}^2$  models.

The models described in this work have been implemented with one of IBM's quantum processors, IBMQ Armonk. All the instructions were compiled and sent to the quantum processor using IBM's Qiskit Pulse package. This presented an opportunity for fine control of microwave pulses applied to the transmon qubit. An important detail of the Qiskit Pulse framework is that it demands that the pulses are not fully continuous, but discretised into small time units of duration  $2/9$  ns. Each transition probability measurement was repeated 2048 times to reduce the impact of random deviations on the final data points. All the pulses used in this work have a temporal pulse area of  $\pi$ , i.e., they are supposed to produce complete population transfer on exact resonance in the absence of decoherence and other losses.

The data was fitted with two different expressions: the analytic formula for the transition probability and a baseline, which was different for each pulse shape:  $B = A \text{sinc}^2(k\Delta) + C$  in the case of the Rabi model and a Lorentzian  $B = A/(1+(k\Delta^2)) + C$  for the rest. The baseline was chosen based on either similarity to the expected transition line profile (as in the Rabi model) or inspired from previously used functions in the literature [12] (as in the Gaussian model).

### III. Pulse shape effects on qubit transition profile

The governing equation for a lossless two-state system is the Schrödinger equation [13] with probability amplitudes  $\mathbf{c}(t) = [c_1(t), c_2(t)]^T$

$$i\hbar \frac{d}{dt} \mathbf{c}(t) = \mathbf{H}(t) \mathbf{c}(t), \quad (5)$$

where  $\mathbf{H}(t)$  is the Hamiltonian,

$$\mathbf{H}(t) = \hbar \begin{bmatrix} 0 & \frac{1}{2}\Omega(t) \\ \frac{1}{2}\Omega(t) & \Delta(t) \end{bmatrix} \quad (6)$$

Here we have assumed the rotating-wave approximation (RWA), where  $\Delta(t)$  is the detuning and  $\Omega(t)$  is the Rabi frequency.

Eq. (6) allows to find exact analytic solutions for different pairs of time-dependent  $\Omega(t)$  and  $\Delta(t)$ . Of these, we select the three available models with a constant detuning,  $\Delta(t) = \text{const}$ . Each of the three models involves a specific time-dependent Rabi frequency, i.e. a specific pulse shape: rectangular (Rabi model), hyperbolic-secant (Rosen-Zener model) and exponential (Demkov model). We also use two other pulse shapes, which do not allow for exact analytic solutions but only approximate ones: Gaussian and squared hyperbolic secant.

#### A. Rectangular pulse: Rabi model

In the Rabi model [7], the Rabi frequency takes a constant form within a finite time interval and is zero outside,

$$\Omega(t) = \begin{cases} \Omega_0, & \text{for } 0 \leq t \leq T; \\ 0, & \text{elsewhere,} \end{cases} \quad (7)$$

where  $T$  is the duration of the pulse, and the detuning  $\Delta$  is constant.

The transition probability reads

$$P_{0 \rightarrow 1}(\Delta) = \frac{\Omega_0^2}{\Delta^2 + \Omega_0^2} \sin^2 \left( \frac{T}{2} \sqrt{\Delta^2 + \Omega_0^2} \right). \quad (8)$$

When plotted versus the detuning the transition probability features a central maximum  $\Omega_0 T = \pi$  and damped oscillations. These oscillations, or satellite peaks, result from the discontinuities at the initial and final instants of the pulse.

The implementation of the Rabi model featured a rectangular pulse applied to the qubit over a time period  $T \approx 501.33$  ns. Since the pulse area must be  $\pi$ , this dictated the choice of the Rabi frequency:  $\Omega_0 \approx 0.9973$  MHz. The corresponding amplitude value in Qiskit was 0.05277. This is the only pulse shape that remains unaffected by the discretisation demanded by Qiskit Pulse, and by the initial and final cut-offs effects, applied to the other pulses.

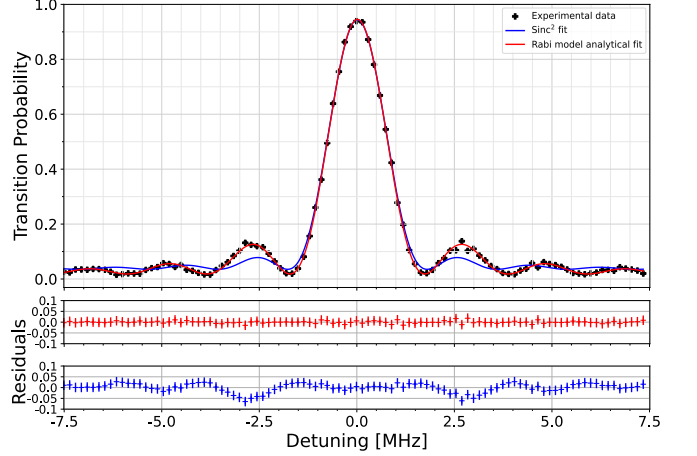


FIG. 1: (Colour online) The transition line profile for the Rabi model: experimental data (black crosses), fit using the Rabi formula (8) (red) and a baseline  $P = \text{sinc}^2(k\Delta)$  curve (blue) for comparison, where  $k$  is a free fitting parameter.

The experimental data and the analytical fits are shown in Fig. 1. The peaks are not well captured by the baseline  $\text{sinc}^2(k\Delta)$  pulse. On the contrary, they are represented very well by the analytical solution for the transition probability of Eq. (8). A plot of the residuals between the analytic (in red) and the baseline (in blue) fits and the experimental data are shown in the bottom of the figure. The divergence indices, obtained by finding the sum of the absolute values of the residuals of the fits, are 0.40 for the analytical fit and 1.55 for the baseline, or nearly a four-fold improvement. Both fits passed the overfitting criterion successfully as the OF parameters were smaller than our empirically chosen limit by a factor of more than 100. The standard deviation of the resonant frequency of the analytical fit was 1.9 kHz compared to 7.3 kHz for the baseline, which is a four-fold decrease of the error bar of the resonant frequency.

#### B. Hyperbolic-secant pulse: Rosen-Zener Model

##### 1. Transition probability

In the Rosen-Zener model [1] the Rabi frequency is a hyperbolic-secant function of time,

$$\Omega(t) = \Omega_0 \operatorname{sech} \left( \frac{t - T/2}{\tau} \right), \quad (9)$$

where  $\tau > 0$  is the pulse width. The detuning  $\Delta$  is constant. The transition probability is given by the exact formula [1]

$$P_{0 \rightarrow 1}(\Delta) = \frac{\sin^2 \left( \frac{1}{2}\pi\Omega_0\tau \right)}{\cosh^2 \left( \frac{1}{2}\pi\Delta\tau \right)}. \quad (10)$$

A unique feature of the Rosen-Zener model is the factorisation of the dependences on the peak Rabi frequency  $\Omega_0$

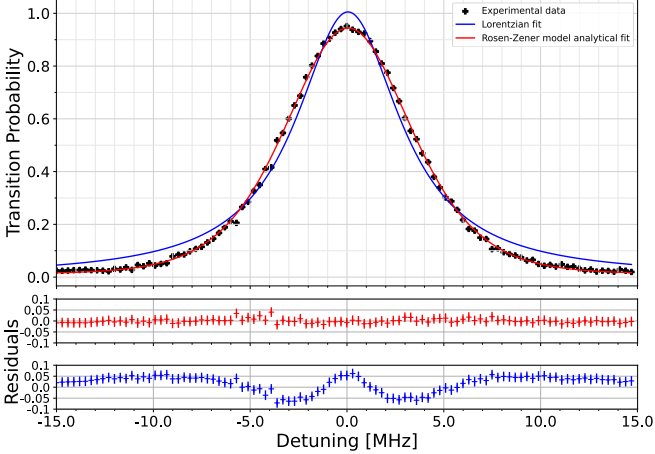


FIG. 2: (Colour online) The transition line profile for the Rosen-Zener model: experimental data (black crosses), fit using the Rosen-Zener formula (10) (red) and a baseline Lorentzian curve (blue) for comparison.

and the detuning  $\Delta$ , a property not found in any other model.

## 2. Implementation

Contrary to the Rabi model, the Rosen-Zener model assumes a pulse of infinite duration. Therefore, we had to truncate the hyperbolic-secant pulse in the experiment. Moreover, unlike the Rabi model, here the discretisation may affect the pulse shape. The pulse that was used had pulse duration (truncation point at)  $T \approx 284.44$  ns and pulse width  $\tau \approx 23.39$  ns, leading to  $\Omega_0 \approx 6.824$  MHz. This constituted a value of 0.3782 for the amplitude given to Qiskit. The experimental data and the analytical fits are shown in Fig. 2. It is evident from the figure that the truncation choice is plausible, since the divergence index improves approximately by a factor of 7 for the model formula (0.69) compared to the Lorentzian baseline (3.64)<sup>1</sup>. Also, it can be noticed from the plot that the tails follow the Rosen-Zener expression almost perfectly, which is reflected in the results. Neither of the two fits is overfit as their OFI are smaller than the threshold by about 2 orders of magnitude.

The standard deviation in the resonant frequency was found to be 11.4 kHz for the analytical fit versus 45.0 kHz for the baseline Lorentzian. Similar to the resonance in the Rabi model, we find that the analytical fit improves the accuracy almost by a factor of 4.

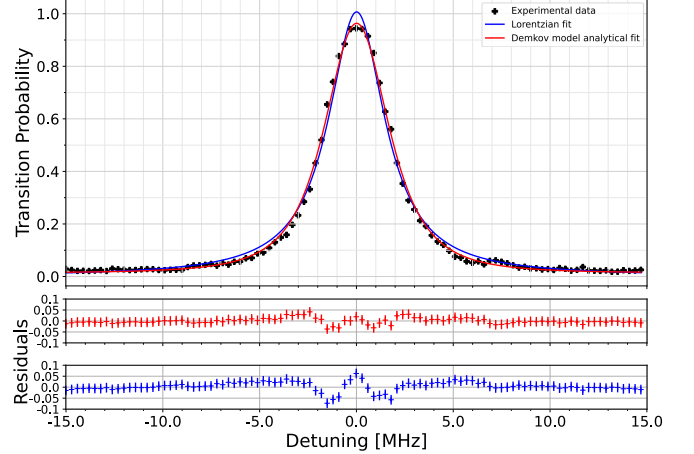


FIG. 3: (Colour online) The transition line profile for the exponential Demkov model: experimental data (black crosses), fit using the analytic formula (12) (red) and a baseline Lorentzian curve (blue) for comparison.

## C. Exponential pulse: Demkov model

### 1. Transition probability

The Demkov model [4] assumes an exponentially varying Rabi frequency,

$$\Omega(t) = \Omega_0 e^{-|t-T/2|/\tau}, \quad (11)$$

and a constant detuning  $\Delta$ . The transition probability for this model is given by the exact expression [14, 15]

$$P_{0 \rightarrow 1}(\Delta) = \left( \frac{\pi \omega}{2} \right)^2 \operatorname{sech}^2 \left( \frac{\pi \delta}{2} \right) \times \left| \operatorname{Re} \left[ J_{(1+i\delta)/2} \left( \frac{\omega}{2} \right) J_{-(1+i\delta)/2} \left( \frac{\omega}{2} \right) \right] \right|^2, \quad (12)$$

where  $J_\nu(z)$  is the Bessel function of the first kind. In this formula  $\delta = \Delta\tau$  and  $\omega = \Omega_0\tau$ .

### 2. Implementation

The implementation on IBM's Armonk system used an exponential pulse of the form (11). The pulse duration was  $T \approx 572.44$  ns and the pulse width was  $\tau \approx 55.56$  ns. The amplitude of the Rabi frequency was  $\Omega_0 \approx 5.052$  MHz, corresponding to an amplitude of 0.2467 in the Qiskit framework. The experimental data and the analytical fits are shown in Fig. 3. We see that the approach to the experiment is also very similar to the one with the Rosen-Zener model. Again, the truncation is not taken into account, and we can see some fine artefacts on the sides of the main resonance peak. One reason for these could be the truncation since no similar effects are predicted by the infinite pulse theory, Eq. (12). The DI for the analytic fit was 0.96, compared

<sup>1</sup> The Lorentzian baseline was inspired from [12] where it is used for fitting Gaussian model resonance peaks.

to 1.50 for the Lorentzian baseline. The DI is once again better for the analytical model, although the two values are comparable, which was not the case in the preceding models.

The reason for the unexpectedly good behavior of the Lorentzian baseline fit, is the cusp-like nonanalyticity of the exponential pulse shape at  $t = 0$ . Indeed, it generates Lorentzian-like behaviour in the tails of the transition line profile [15], which make it similar to the baseline fit.

Other than that effect, the error bar of the resonance frequency was decreased by a factor of 1.6 using the analytic fit: from 17.6 kHz to 11.7 kHz. The behaviour is expected and both fits pass the overfitting criterion.

#### D. Gaussian pulse

##### 1. Transition probability

So far we have only considered exact analytic solutions for the models. For the Gaussian model we have the Rabi frequency

$$\Omega(t) = \Omega_0 \exp \left( -\frac{(t - T/2)^2}{2\tau^2} \right) \quad (13)$$

and we use an approximate analytical model for the transition probability [2]. The model can be solved using the Davis-Pechukas approach [2] yielding the following expression for the transition probability

$$P_{0 \rightarrow 1}(\Delta) = \frac{\sin^2 [\operatorname{Re}(\mathcal{D}(\Delta; \tau_0^+))]}{\cosh^2 [\operatorname{Im}(\mathcal{D}(\Delta; \tau_0^+))]}, \quad (14)$$

where

$$\mathcal{D}(\Delta; \tau_0^+) = \Delta T \int_0^{\tau_0^+} \sqrt{\alpha^2 e^{-2\tau^2} + 1} d\tau, \quad (15)$$

is the Davis-Pechukas integral for the first transition point  $\tau_0^+$ , which is the first (complex-valued, in the upper half-plane) root of the quasienergy splitting  $\varepsilon(t) = \sqrt{\Omega^2(t) + \Delta^2}$ . The resulting values for the real part of the Davis-Pechukas integral are

$$\begin{aligned} \operatorname{Re}(\mathcal{D}(\Delta; \tau_0^+)) \approx \Delta T & \left\{ \left( \sqrt{\alpha^2 + 1} \right) - 1 \right. \\ & \times \sqrt{\frac{1}{2} \ln \left( \frac{\alpha^2}{((1 + \nu(\sqrt{\alpha^2 + 1} - 1))^2 - 1)} \right)} \\ & \left. + \frac{1}{2} \sqrt{\sqrt{(L^2 + \pi^2)} + L} \right\}, \end{aligned} \quad (16)$$

where

$$L = \ln \left( \frac{\alpha^2}{\mu(2 - \mu)} \right),$$

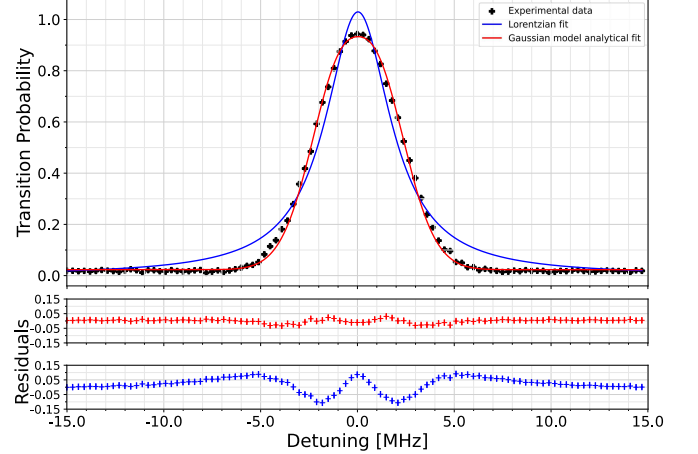


FIG. 4: (Colour online) The transition line profile for the Gaussian model: experimental data (black crosses), fit using the Gaussian model approximate formula (14) (red) and a baseline Lorentzian curve (blue) for comparison.

$\alpha = \Omega_0/\Delta$ ,  $\mu \approx 0.316193$  and  $\nu \approx 0.462350$  are constants. The imaginary part of the Davis-Pechukas integral is

$$\operatorname{Im}(\mathcal{D}(\Delta; \tau_0^+)) \approx \frac{1}{2} \Delta T \sqrt{\sqrt{4 \ln^2(m\alpha) + \pi^2} - 2 \ln(m\alpha)}, \quad (17)$$

where  $m \approx 1.311468$  is a constant [2].

##### 2. Implementation

For this analysis a pulse with duration  $T \approx 398.22$  ns and width  $\tau \approx 49.78$  ns was used. Because all pulses in this work had an area of  $\pi$  we found the Rabi frequency amplitude  $\Omega_0 \approx 4.007$  MHz. The equivalent value for the amplitude fed to the Armonk system was 0.2195. The experimental data and the analytical fits are shown in Fig. 4. The results suggest that the approximate expression (14) is in better agreement with the experiment than the Lorentzian baseline. The divergence indices are 0.89 for the approximate model versus 4.02 for the Lorentzian baseline, which signals a reduction of the DI by a factor of 4.5 using our fit. This confirms the relevancy of the approximate solution [2].

The standard deviation of the resonance frequency found with the analytic model was 10.7 kHz, compared to 43.9 kHz for the baseline, or approximately a decrease of the error by a factor of 4. The OFI indices of the two fits are also well within the overfitting threshold.

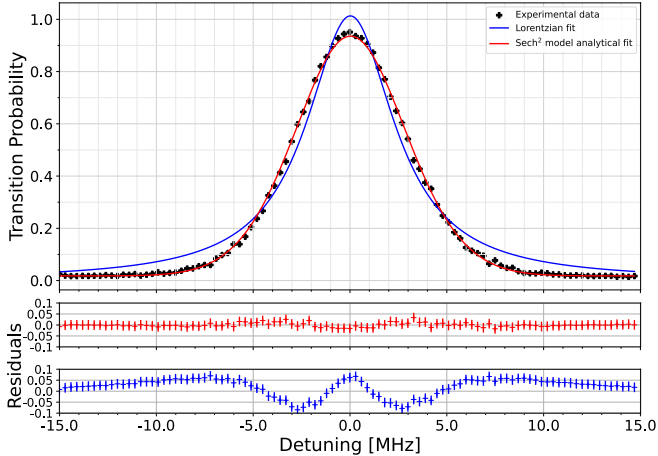


FIG. 5: (Colour online) The transition line profile for the  $\text{sech}^2$  model: experimental data (black crosses), fit using the  $\text{sech}^2$  model formula (Eq. (20)) (red) and a baseline Lorentzian curve (blue) for comparison.

### E. Squared hyperbolic-secant pulse: the $\text{sech}^2$ model

#### 1. Transition probability

The  $\text{sech}^2$  model is another model which has no exact analytic solution. The Rabi frequency takes the shape

$$\Omega(t) = \Omega_0 \text{sech}^2\left(\frac{t - T/2}{\tau}\right), \quad (18)$$

and the detuning  $\Delta$  is constant. The analytical form of the transition probability was derived using the Fourier transform formula first conjectured by Rosen and Zener [1], and later modified in [16]. The transition probability  $P_{0 \rightarrow 1}$  is given by

$$P_{0 \rightarrow 1}(\Delta) = \sin^2(S/2) \left| \frac{1}{\Omega_0 \tau} \int_{-\infty}^{\infty} \Omega(t) e^{i\Delta t} dt \right|^2. \quad (19)$$

Using Eqs. (18) and (19) and assuming that  $\tau > 0$  and  $\Delta$  are real we solve the integral and find that

$$P_{0 \rightarrow 1}(\Delta) = \frac{(\pi \Delta \tau)^2 \sin^2(\frac{1}{2}S(\Delta))}{\sinh^2(\frac{1}{2}\pi \tau \Delta)}. \quad (20)$$

It is important that in Rosen and Zener's paper [1] the pulse area is  $S = \Omega_0 \tau$ , but in this work we use a modification of the form  $S(\Delta) = \tau \sqrt{\Omega_0^2 + a\Delta^2}$ , as shown in [10, 16]. Here  $a$  is a free parameter that depends on the pulse shape. Its value is 0 for the Rosen-Zener model and 1 for the Rabi model [10]. By fitting the approximate expression (20) to the numerical solution of the Schrödinger equation we fix the value  $a = 0.449$ .

### 2. Implementation

Experimentally, the  $\text{sech}^2$  model was implemented on the IBMQ Armonk quantum computer using a discretised form of the pulse shape (18). The duration of the pulse (truncation point) was  $T \approx 284.44$  ns and the pulse width was  $\tau \approx 44.44$  ns. The value for the Rabi frequency amplitude was  $\Omega_0 \approx 5.644$  MHz. This is equivalent to an amplitude of 0.3149 in the Qiskit package.

The experimental data and the analytical fits are shown in Fig. 5. The analytical formula matches the measured values far better than the Lorentzian fit, resulting in a smaller value for the divergence index: 0.65 for the formula versus 4.03 for the baseline fit, or more than a 6-fold improvement. However, a certain inconsistency can be noticed in the width of the analytical profile, compared to the experimental data. A strong improvement in the resonance frequency was made, as the standard deviation of the resonant value was decreased nearly by a factor of 5 — from 45.6 kHz to 9.9 kHz. No overfitting was detected in either of the fits.

### F. Discussion

The values of the divergence index (DI) and the standard deviation of the resonance frequency (SDRF) for all models are summarized in Table I. For all models the reduction of both DI and SDRF is by a factor of 4 to 7. The only exception is the exponential Demkov model for which the improvement is about 60% due to the nonanalyticity of the pulse shape at its maximum, which makes the Lorentzian fit quite reasonable, as discussed in Sec. III C. Yet, in absolute terms (i.e. disregarding the baseline fits), the analytic fit for the Demkov model is nearly as good as those for the other analytic models, delivering comparable values of the DI.

We also note the fact that the Rabi model gives the best value of the DI compared to the other models. We trace the reason for this to the fact that all other pulses are truncated at times 0 and  $T$ , and this truncation is not reflected in the analytic formulas used by us.

The Rabi model also offers the best values of the SDRF. This derives from the fact that it has the longest pulse width (501.33 ns) compared to values  $\tau$  in the range from 23 to 56 ns for the other 4 models. (Consequently, the Rabi model used the smallest value of the peak Rabi frequency (0.9973 MHz), whereas for the other models Rabi frequencies larger by a factor of 4 to 7 have been used.)

### IV. Conclusion

We have presented experimental results of the measurement of the qubit transition line profiles for five different pulse shapes of the driving microwave field obtained using one of the online IBM quantum processors.

Model	Analytic DI	Baseline DI	Analytic SDRF (kHz)	Baseline SDRF (kHz)
Rabi	0.40	1.55	1.9	7.3
Rosen-Zener	0.69	3.64	11.4	45.0
Demkov	0.96	1.50	11.7	17.6
Gaussian	0.89	4.02	10.7	43.9
Sech <sup>2</sup>	0.65	4.03	9.9	45.6

TABLE I: Values for the divergence index (DI) and the standard deviation of the resonance frequency (SDRF) for each of the models, including the value for the baseline fit.

We have compared these experimental profiles with two types of fits: one using the exact or approximate analytic solution for the respective pulse shape and the other using the routinely exploited Lorentzian or  $\text{sinc}^2$  functions. We have shown that the experimental data show much better resemblance to the respective analytic solutions than to intuitive fitting functions, according to our custom divergence indices (DI) (see Table I). Nevertheless, we have outlined some minor inconsistencies due to unavoidable the truncation of the driving pulse amplitude. For all but the exponential model the DI index shows an improvement by a factor of 4 to 7. For the exponential model the improvement is by some 60% only, because the (Lorentzian) baseline behaves much better than for the sech,  $\text{sech}^2$  and Gaussian models. The reason can be traced to the non-analyticity of the Demkov model, which, like the rectangular pulse, generates Lorentzian-like artefacts in the excitation profile. Coincidentally, these artefacts fit with the fat tail of the baseline fit.

Such a comparison provides quantitative measures of both the accuracy of the respective theoretical model, the quality of the driving field, and the “quantumness” of the qubit regarding its coherence properties.

Apart from demonstrating fine features of qubit dynamics, the results in this paper can have an useful practical application: more accurate determination of the exact resonance, which can result in improved fidelity of the quantum gates. For the five pulse shapes studied here, we have found differences in the resonant frequency, as determined by the analytic formulae and the baseline fits, in the range of a few dozens of kHz. The superiority of the new values for the resonant frequency has been verified by a reduction of its standard deviation by a factor of about 4 in 4 of the models; the only exception to this was the Demkov model, where the error was reduced by a factor of 1.6. This difference may affect the fidelity of the quantum gates, especially for longer pulse durations. Therefore, the present paper provides an easy solution to one of the experimental issues in the quest for ultrahigh fidelity of gate operations.

Finally, although the results in this paper have been demonstrated on a specific quantum computing platform — the transmon-based IBM Quantum system — the conclusions should be generally valid on any other physical platform.

## Acknowledgments

This research is supported by the Bulgarian national plan for recovery and resilience, contract BG-RRP-2.004-0008-C01 (SUMMIT), project number 3.1.4.

### A. Two-state transmon physics

Any purely two-level quantum system is a qubit (e.g. the electron spin). However, in practice some multi-level systems are also used as two-level systems. The main condition is that there is sufficient anharmonicity present, which allows the transitions between the first two levels to be controlled independently from the next possible transition. In other words, the anharmonicity is the difference between the energy of the  $0 \rightarrow 1$  and the  $1 \rightarrow 2$  transitions [17]. One system which satisfies the “qubit requirements” is the transmon, which is formulated from *transmission-line shunted plasma oscillation qubit* [18].

In order to explain its physics, it is easier to start with a normal LC circuit and derive the Hamiltonian for it, before we jump into the transmon. The Hamiltonian for a normal LC circuit is equivalent to the one for a linear harmonic oscillator if we express the mass  $m$  for the capacitance  $C$ , the momentum  $p$  for the electrical charge  $Q$  and the resonant frequency  $\omega_r = 1/\sqrt{LC}$ . Therefore, the usual Hamiltonian for the linear harmonic oscillator reads

$$\mathcal{H}_{LHO} = \frac{p^2}{2m} + \frac{m\omega^2 x^2}{2} \quad (\text{A1})$$

becomes

$$\mathcal{H}_{LC} = \frac{Q^2}{2C} + \frac{\Phi^2}{2L} = \frac{1}{2}CV^2 + \frac{1}{2}LI^2 \quad (\text{A2})$$

where  $\Phi$  is the magnetic flux,  $I$  is the electric current,  $L$  is the inductance and  $V$  is the voltage [17].

We can also introduce non-linear versions of the charge and the flux - the reduced charge  $n = Q/(2e)$ , where  $e$  is the electron charge, and the reduced flux  $\phi = 2\pi\Phi/\Phi_0$ , with  $\Phi_0 = h/(2e)$  being the magnetic flux quantum [17]. Then we substitute the linear charge and flux in Eq. (A2) and yield

$$\mathcal{H}_{LC} = \frac{4en^2}{2C} + \frac{\Phi_0^2\phi^2}{8\pi^2L}. \quad (\text{A3})$$

The constants in front of  $n$  and  $\phi$  can be simplified by introducing

$$E_C = \frac{e^2}{2C} \text{ and} \\ E_L = \frac{\Phi_0^2}{4\pi^2L}, \quad (\text{A4})$$

where  $E_C$  is the charging energy needed to add another Cooper pair to the island, and  $E_L$  is the inductive energy.

Then we obtain an equation for the Hamiltonian in terms of these constants which reads

$$\mathcal{H}_{LC} = 4E_C n^2 + \frac{1}{2}E_L \phi^2. \quad (A5)$$

To some extent, the transmon is similar to the plain LC circuit, but instead of the inductance we have a so-called Josephson junction [19, 20]. This is a non-linear circuit element that does not allow any dissipation, and essentially acts as a non-linear version of the inductance. To find the transmon Hamiltonian  $H_T$ , we need to incorporate its properties into the equation. Its properties are best described by the identities for  $I$  and  $V$

$$I = I_c \sin(\phi), \quad V = \frac{\hbar}{2e} \frac{d\phi}{dt}. \quad (A6)$$

These expressions yield

$$\mathcal{H}_T = 4E_\Sigma n^2 + E_J \cos \phi \quad (A7)$$

for the transmon Hamiltonian, with

$$E_\Sigma = \frac{e^2}{2C_\Sigma}, \quad E_J = \frac{I_c \Phi_0}{2\pi}, \quad (A8)$$

where  $C_\Sigma = C_s + C_J$  is formed by both the shunt capacitance  $C_s$  and the self-capacitance  $C_J$  of the Josephson junction. The second term in Eq. (A7) is nonlinear but it can be Taylor expanded for small values of  $\phi$ . This results in

$$E_J \cos(\phi) = E_J - \frac{1}{2}E_J \phi^2 + \frac{1}{24}E_J \phi^4 - \mathcal{O}(\phi^6), \quad (A9)$$

where we retain only the first three terms. The second term is quadratic and if we limit ourselves there, we would be looking at a quantum harmonic oscillator (QHO). However, the third term is quartic in  $\phi$  and

it is responsible for the uneven shift in energy levels and the resulting differences in excitation energies between them (the anharmonicity). It is also clear from the sign of the third term that the anharmonicity  $\alpha = E_{1 \rightarrow 2} - E_{0 \rightarrow 1}$  is negative and the transition energy decreases for the higher levels.

The energy contributions by the charge and the flux parts are determined by the ratio  $E_J/E_\Sigma$ . Experimentally, it was found that flux noise was much easier to control than charge noise. If  $E_J \ll E_\Sigma$  the qubit became much more sensitive to charge noise, so this was ruled out. Instead, a suitable value for the ratio was found to be  $E_J/E_\Sigma \gtrsim 50$  [21–24]. The methods to achieving such a ratio mainly aim at reducing  $E_\Sigma$  by having a capacitor with high capacitance, effectively decreasing charge noise. That is the case in the transmon qubit [18].

By taking the three leading terms in the Taylor expansion of Eq. (A9), we can express the Hamiltonian in its second quantisation form as

$$H_T = E_0 a^\dagger a + \frac{\alpha}{2} a^\dagger a^\dagger a a, \quad (A10)$$

where  $|\alpha| \ll E_0$  which is consistent with an anharmonic oscillator. If  $|\alpha|$  is large enough and gates are constructed so as to prevent leakage (as in the so-called DРАG gates [25]), excitation to higher levels is suppressed and we can effectively treat the system as a two-level quantum system. The Hamiltonian can be reduced to

$$H_T = E_0 \frac{\sigma_z}{2}, \quad (A11)$$

where  $\sigma_z = \text{diag}(1, -1)$  is the corresponding Pauli matrix. As long as the  $E_J/E_\Sigma \gtrsim 50$  condition holds, we have a functional superconducting qubit.

---

[1] N. Rosen and C. Zener, Phys. Rev. **40**, 502 (1932).  
[2] G. S. Vasilev and N. V. Vitanov, Phys. Rev. A **70**, 053407 (2004).  
[3] L. S. Simeonov and N. V. Vitanov, Phys. Rev. A **89**, 043411 (2014).  
[4] Y. N. Demkov, Sov. Phys. JETP **18**, 138 (1963).  
[5] I. I. Boradjiev and N. V. Vitanov, Phys. Rev. A **88**, 013402 (2013).  
[6] G. S. Vasilev and N. V. Vitanov, arXiv:1402.5119 (2014).  
[7] I. I. Rabi, Phys. Rev. **51**, 652 (1937).  
[8] N. Vitanov, B. Shore, L. Yatsenko, K. Böhmer, T. Halfmann, T. Rickes, and K. Bergmann, Opt. Commun. **199**, 117 (2001), ISSN 0030-4018.  
[9] T. Halfmann, T. Rickes, N. V. Vitanov, and K. Bergmann, Opt. Commun. **220**, 353 (2003), ISSN 0030-4018.  
[10] C. W. S. Conover, Phys. Rev. A **84**, 063416 (2011).  
[11] Compute resources, URL <https://quantum-computing.ibm.com/services/resources?services=systems>.  
[12] A. Abbas, S. Andersson, A. Asfaw, A. Corcoles, L. Bello, Y. Ben-Haim, M. Bozzo-Rey, S. Bravyi, N. Brönn, L. Capelluto, et al., *Learn quantum computation using qiskit* (2020), URL <https://qiskit.org/textbook/>.  
[13] B. W. Shore, The Theory of Coherent Atomic Excitation, Volume 1, Simple Atoms and Fields, by Bruce W. Shore, pp. 774. ISBN 0-471-61398-3. Wiley-VCH, July 1990. (1990).  
[14] N. V. Vitanov and G. Panay, J. Phys. B At. Mol. Opt. Phys. **25**, 239 (1992).  
[15] N. V. Vitanov, J. Phys. B At. Mol. Opt. Phys. **26**, L53 (1993).  
[16] R. T. Robiscoe, Phys. Rev. A **27**, 1365 (1983).  
[17] P. Krantz, M. Kjaergaard, F. Yan, T. P. Orlando, S. Gustavsson, and W. D. Oliver, Appl. Phys. Rev. **6**, 021318 (2019).  
[18] J. Koch, T. M. Yu, J. Gambetta, A. A. Houck, D. I. Schuster, J. Majer, A. Blais, M. H. Devoret, S. M. Girvin, and R. J. Schoelkopf, Phys. Rev. A **76**, 042319 (2007).

- [19] B. Josephson, Phys. Lett. **1**, 251 (1962), ISSN 0031-9163.
- [20] B. D. Josephson, Rev. Mod. Phys. **36**, 216 (1964).
- [21] Y. Nakamura, Y. A. Pashkin, and J. S. Tsai, Nature **398**, 786 (1999).
- [22] D. Vion, A. Aassime, A. Cottet, P. Joyez, H. Pothier, C. Urbina, D. Esteve, and M. H. Devoret, Science **296**, 886 (2002).
- [23] J. Q. You and F. Nori, Phys. Rev. B **68**, 064509 (2003).
- [24] T. Duty, D. Gunnarsson, K. Bladh, and P. Delsing, Phys. Rev. B **69**, 140503 (2004).
- [25] M. Werninghaus, D. J. Egger, F. Roy, S. Machnes, F. K. Wilhelm, and S. Filipp, NPJ Quantum Inf. **7**, 14 (2021).